Volume 48(2): 295–302, 2000
The Journal of Histochemistry & Cytochemistry
http://www.jhc.org

TECHNICAL NOTE

PS-100 and NF 70-200 Double Immunolabeling for Human Digital Skin Meissner Corpuscle 3D Imaging

Didier Guinard, Yves Usson, Christiane Guillermet, and Raymond Saxod

Equipe de Neurobiologie du Développement LAPSEN-U Inserm 318, Université Joseph Fourier (DG); TIM C UMR 5525 CNRS, Institut Albert Bonniot, Université Joseph Fourier (YU); Laboratoire de Pathologie Cellulaire, Centre Hospitalier Universitaire de Grenoble (CG); and Equipe de Neurobiologie du Développement LAPSEN-U Inserm 318, Université Joseph Fourier (RS), Grenoble, France.

SUMMARY For detailed study of complex structures such as corpuscular mechanoreceptors, confocal microscopy can be used with multiple immunolabeling that identifies specifically different subcomponents. In addition, anatomic interpretation is enhanced by three-dimensional reconstruction. Confocal laser micrographs, reconstructed from serial images 1 μm thick of human skin Meissner corpuscles simultaneously immunostained for neurofilaments (NF 70-200) and protein S-100 (PS-100), clearly reveal the complex 3D relationship between Schwann-related lamellar cells immunoreactive for PS-100 and the nerve fibers marked by NF 70-200. The nerve fiber, after branching into the corpuscle, divides into several ramifications, presenting discoidal expansions and flattened fringed sections. The mean nerve diameter was 4 μm ± 1 (2–5 μm) and the mean size of the discoidal expansions was 15 μm ± 1 (7–30 μm). Corpuscle size varied from 30–140 ± 1 μm in length and from 20–60 ± 1 μm in diameter. This study confirms the presence of neural discoidal areas in Meissner's corpuscles, which are probably involved to some extent with the transduction process. Despite the accuracy of immunolabeling and imaging, an extracorpuscular neural network was never observed in the vicinity of corpuscles, thus giving doubt as to their existence. **(J Histochem Cytochem 48:295–302, 2000)**

KEY WORDS
Meissner corpuscles
immunolabeling
confocal microscopy
mechanoreceptors
3D reconstruction
cutaneous innervation
finger

Since its first description, our understanding of the architecture of the Meissner's corpuscle has been enhanced by studies at the optical level (LM) and with transmission electron microscopy (TEM) (Cauna 1956a,b; Cauna and Ross 1960; Chouchkov 1973; Castano 1974; Halata 1975; Breatnach 1977; Matsuoka et al. 1983). A tortuous organization of the spiral nerve course with the interlaced stack of Schwann-related lamellar cells has been described in mammalian and human skin with specific variations according to species (Idé 1976; Ventura and Castano 1977; Castano and Ventura 1978,1979; Castano et al. 1985; Munger and Idé 1988; Saxod 1996). However these studies have provided little information about the overall spatial arrangement or the relationship between morphology and function.

At present, immunolabeling techniques are the most reliable means for identifying neural structures. Of the many neuropeptides and proteins that have been reported in sensory endings, protein S-100 (PS-100) has proved to be a reliable marker of Schwann cells, and nerve fibers are labeled specifically by antibodies against neurofilaments (NF 70, NF 70-200) (Iwanaga et al. 1982; Stefansson et al. 1982; Dalsgaard et al. 1984; Hachisuka et al. 1984; Björklund et al. 1986; Haro et al. 1991; Karanth et al. 1991; Ramieri et al. 1992; Kennedy and Wendelschafer–Crabb 1993).

For complex structures such as corpuscular mechanoreceptors, simultaneous specific labeling by different markers allows better identification of the different substructures, thus improving anatomic interpretation (Dubövy et al. 1993; Vega et al. 1996). At present, acquisition of serial optical sections by confocal laser

Correspondence to: D. Guinard, Equipe de Neurobiologie du Développement, LAPSEN-U Inserm 318, Université Joseph Fourier, BP 217, 38043 Grenoble Cedex 9, France.

Received for publication June 4, 1999; accepted September 29, 1999 (9T4997).

0022-1554/00/$3.30

scanning microscopy (CSLM) combined with three-dimensional (3D) reconstruction techniques provides high-contrast images that depict microscopic anatomy more realistically than was previously possible (Mayhew 1992; Castano et al. 1993,1995; Rumio et al. 1995b). In addition, with appropriate software, image analysis is improved by the possibility of virtual rotation of the object in space, allowing observation of the reconstruction in toto from any desired viewpoint (Cheng and Summers 1990; Carlsson 1991; Parazza et al. 1993). This study used double immunolabeling and CSLM to investigate Meissner corpuscles in human fingers.

Materials and Methods

Tissue Preparation

Human digital pulps of two second digits were obtained from non-replantable traumatic amputations on the dominant hand of two manual workers (43 and 51 years old) without medical antecedents who gave their informed consent in accordance with the Helsinki Declaration of 1975. Samples were immediately excised and fixed with 4% formaldehyde in pH 7.4 PBS 0.01 M for 24 hr at 4C. After rinsing in distilled water, pulp tissue was cut into small fragments perpendicular to the skin surface ($1 \times 6 \times 3$ mm) and immediately embedded in agar or paraffin. Thick serial sections (70 μm) were made from agar-embedded samples with a vibratome (Vibraslice 752 M; Campden Instruments, Oxford, UK) and treated for immunolabeling. Thin (7-μm) sections for conventional light microscopy were cut from paraffin-embedded samples with a microtome (Reichert–Jung 2050 Microm; Vienna, Austria).

Immunofluorescence and Immunochemistry

Agar-embedded samples were labeled using a floating technique. To enhance marker penetration, samples were pretreated by microwaving (Micromat 120 AEG; frequency 2.45 Hz, 850 W) in a 0.01 M pH 6 sodium citrate buffer (three sessions of 5 min each). After incubation in 0.01 M PBS with 2% skimmed milk powder at 4C for 1 hr and rinsing, primary antibodies were applied for 48 hr at 4C in a humid atmosphere with gentle agitation. Immunolabeling was performed with murine monoclonal antibodies (clone 2F11) to NF 70-200 (Chemical Credential; Costa Mesa, CA) at a dilution of 1:100 and with rabbit polyclonal antibodies to PS-100 (Immunotech 1071; Marseille, France) at a dilution of 1:48. After rinsing in 0.01 M PBS, pH 8.6 (three times for 20 min) and incubation in 1% bovine serum albumen (BSA) for 30 min, a second rinse in 0.01 M PBS, pH 8.6 (three times for 20 min) was done. Secondary fluorescence-conjugated antibodies were sequentially applied at 4C in a humid and dark atmosphere for 3 hr with 0.01 M PBS, pH 8.6 (1 hr) and 1% BSA (30 min) rinses between the two sequences as follows: first 1:100 rhodamine-conjugated (TRITC) goat anti-rabbit antibodies (Jackson; West Grove, PA) were used to recognize NF 70-200 and then 1:75 fluorescein-conjugated (FITC) rabbit anti-murine antibodies (Dako; Glostrup, Denmark) were applied to identify PS-100. After rinsing in 0.01 M PBS, pH 8.6 (1 hr), samples were mounted in an antifading medium (0.05 M Tris-HCl, 8%, pH 7.6, glycerol (90%), 1.4 diaziabyclo-octan (2%) (Sigma, St Louis, MO; D 2522) between a slide and a coverslip sealed with nailpolish. Control sections were prepared by substituting normal serum for primary antibodies or by eliminating the first incubation.

For light microscopy, thin sections were treated with the same immunochemical process as described above for PS-100 antibodies (Immunotech 1071). Specific staining was revealed by incubation with biotinylated donkey anti-rabbit antibodies (Jackson) followed by a peroxidase-conjugated avidin–biotin complex (1: 400, PBS 7.4, BSA 1%, 1 hr) (StreptABComplex/HRP; Dako) and diaminobenzidine tetrachloride baths. Counterstaining of cell nuclei was performed with hematoxylin.

Confocal Microscopy

Confocal optical sections were collected with a confocal scanning laser microscope LSM 410 Invert (Carl Zeiss; Oberkochen, Germany) using a ×40 objective lens (Plan-Neofluoar, 1.3 NA, oil immersion). Simultaneous imaging of FITC and TRITC fluorescence was performed with the following settings. Both labels were excited with the 488-nm line of an argon laser while the excitation beam was separated from emitted fluorescence by a 510-nm dichroic mirror. The two fluorescences were segregated with a 560-nm beam separator and respectively selected with a 520–560-nm bandpass filter (FITC spectrum) and a 590-nm longpass filter (TRITC spectrum). The signal-to-noise ratio was improved by averaging eight ordered frames for each optical section. During the scanning session, correction of attenuation of emitted and reflected light due to sample penetration was accomplished by gain compensation of the photomultiplier (voltage magnification). Neither fluorescence bleached appreciably even during long exposures (up to 15 min/50 optical sections).

Tridimensional Reconstruction

The stacks of confocal images were edited, processed, and reconstructed with the Edit3D software developed in our laboratory (Parazza et al. 1993). This program runs on various computer platforms and operating systems: SGI workstations (IRIX 5.x,6.x), PowerMacintosh microcomputers (MacOS and LinuxPPC), and Intel PCs under Linux.

Processing

After collecting the confocal series, it was necessary to process these data to correct for image degradation inherent to confocal microscopy. Two main image artifacts were taken into account: (a) poor signal-vs-noise ratio (SNR) and (b) loss of fluorescence intensity as we penetrated deeper inside the thick tissue sections.

A 3D median filter was used to reduce the noise. This filter has the property of removing "salt and pepper" noise while preserving edge information in images. It uses a $3 \times 3 \times 3$ window centered on the voxel (volume element) to be filtered, sorts the intensities of the voxels within the window, and returns the median value. This median intensity

value is then substituted to the original value of the current voxel.

Although the biological samples are usually transparent they tend to absorb and scatter a small amount of light. In tissue sections in which thickness is greater than 5 μm, the absorption phenomenon is no longer negligible. On the one hand, the excitation light is gradually attenuated as a function of depth on the way in. On the other hand, the emitted light is also attenuated on the way out. This results in a real decrease in the signal intensity as a function of Z. The curve of attenuation of fluorescence intensity as a function of depth can be modeled by a log-logistic function (Rigaut and Vassy 1991). The correction consisted of multiplying the intensities of the voxels by a coefficient whose value increased with depth according to the following formula:

$$I_z' = I_z\left[\left(\frac{Z_{\max}}{K}\right)^a - \left(\frac{Z_{\max} - Z}{K}\right)^a\right]$$

with Z the current depth, Z_{max} the deepest section of the series, I_z the voxel intensity at current depth, and I_z' the new voxel intensity. K and a are empirically defined constants.

Reconstruction

Different visual attributes of the 3D reconstruction can be selected to best visualize specific details. According to the needed attributes (shape or content of the object), a surface or a transparency-rendering approach can be used. Surface rendering is obtained by simulating bundles of parallel rays of light traversing the pixels (elementary points) of the viewing screen of the computer. When one of these rays hits a surface voxel of an object (e.g., nerve fibers), the intensity of the corresponding screen pixel was modulated as a function of the cosine of the angle between the incident ray and the normal to the object surface at the hit spot. The voxels of the object were first obtained by applying a simple intensity threshold rule: All voxels whose intensity is greater than the given value are considered to belong to the object. The other voxels are labeled as background.

In contrast to the surface model in which only the surface voxels are considered, the volume model is intended to show all the information contained in the 3D cube. This display mode might be called "see-through" or transparent viewing. The method for representing transparent volumes is called "ray casting." It consists of dividing the viewing screen into small pixels. Then we consider that each pixel of the viewing screen receives a ray of light that originated from infinity and that traversed the 3D data volume. The intensity of a given ray is the result of the information encountered along its path. In other words, the light intensities of all the traversed voxels are accumulated and contribute to the brightness and color of the pixel displayed on the screen.

Results

As deduced previously with conventional histological techniques, 3D reconstruction and double immunolabeling show the characteristic organization of Meissner corpuscles with a complicated interweaving of the helical nerve fiber winding within the stacks of lamellar cells, forming a spring-like framework (Figures 1A–1C). Corpuscles are usually found alone or grouped in a dermal papilla, with their long axis vertically oriented (Figure 1A). Lamellar cells are highly immunoreactive for PS-100 and are well differentiated from the nerve component labeled by antibodies against NF 70-200 (Figures 1C–1D and 2A–2B). The afferent nerve fiber can be followed along its extra- and intracorpuscular course. A single extracorpuscular nerve fiber can branch into several sensory endings (Figures 2A and 2B). Each corpuscle is penetrated through its base by dividing nerve ramifications which run in an helical fashion (Figures 2C–2D). The nerve fiber presents flat, discoidal, more or less fringed regions randomly situated along the nerve course, usually one per corpuscle (Figure 2E). These formations are not easily noticeable on single optical sections and are better appreciated after 3D reconstruction, particularly when the "nerve fluorescence channel" (NF 70-200) is observed alone (Figures 2C–2D).

On the other hand, labeled lamellar cells, which are arranged in stacks intercalated with the tortuous annulospiral nerve course, are more evident on a single optical section (Figure 1C) than in a 3D reconstruction, in which they have a more diffuse appearance (Figures 2A and 2B). During tomography sessions, the use of only one laser beam (argon) that activates both FITC and TRITC labels provides no blurring of the image. In addition, appropriate object rotation provides vision from another angle which modifies and corrects image interpretation (Figure 2E). Apparent discontinuities are probably artifacts caused by incomplete labeling of the sample or by photonic reflection defaults rather than a real structural defect (Figures 2A and 2B). Despite the quality of labeling that is sufficient to distinguish fibers with diameters of less than 0.8 μm, no extracorpuscular network has been identified in the vicinity of observed corpuscles (Figures 2A–2D). Measurements whose mean and SEM refer only to the optical 3D resolution give a nerve diameter that varies from 2 to 5 μm (mean diameter 4 ± 1 μm), with size differences which are more easily appraised on a stereoscopic view (Figures 2C–2D) whereas discoidal expansions have a mean diameter of 15 ± 1 μm (from 7 to 30 μm) (Figure 2E). Corpuscle size, measured from five samples (not shown), varies from 30 to 140 ± 1 μm in length and from 20 to 60 ± 1 μm in diameter.

Discussion

This study shows that double immunolabeling of thick samples observed by confocal microscopy allows reliable imaging of Meissner corpuscles. Many LM and TEM studies have demonstrated their fine structure, but analysis of this sophisticated framework could re-

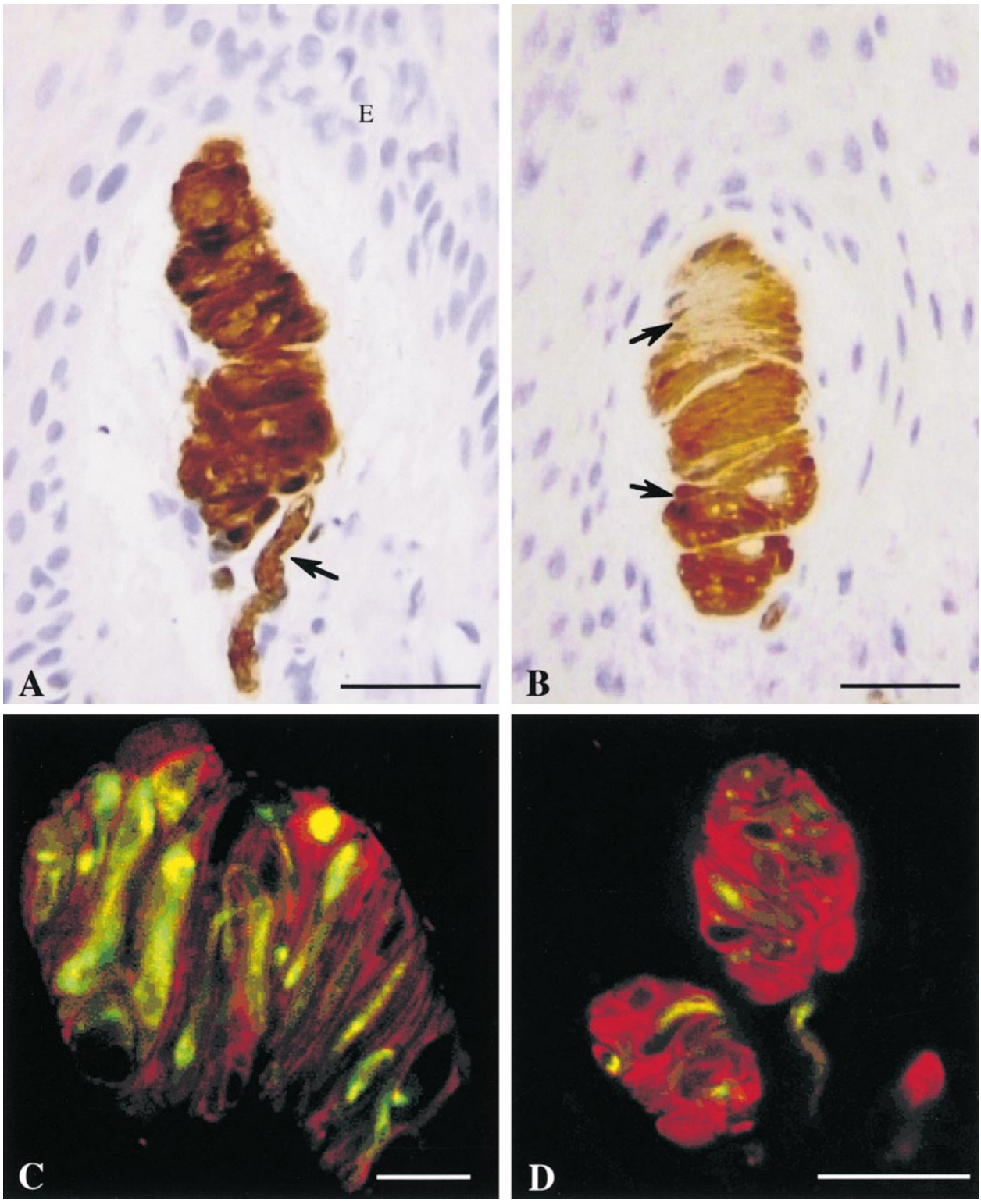

Figure 1 (**A**) Meissner corpuscles labeled with anti-PS-100 antibodies (peroxidase immunostaining). The complex spiral organization is evident. The corpuscle is connected to an afferent nerve at its basal extremity (arrow). The corpuscle is oriented vertically in a dermal papilla. E, epidermis. Thin paraffin sections (7 μm) of human digital pulp. Hematoxylin counterstaining. Light microscopy. Bar = 40 μm. (**B**) The organization of lamellar cells in a Meissner corpuscle. Arrows indicate nuclei of lamellar cells. Same parameters as in **A**. (**C**) Optical section (CSLM, laser argon 488 nm) of a double fluorescent-conjugated immunolabeled Meissner corpuscle. The double and distinct labeling allows a clear appreciation of the tortuous spiral nerve course (NF 70-200, yellow-green). Lamellar Schwann cells (PS-100, red) appear in stacks, and

main difficult (Cauna 1956a,b; Cauna and Ross 1960; Chouchkov 1973; Haschimoto 1973; Castano 1974; Iggo 1974; Halata 1975; Breatnach 1977). Reconstructions from 2D serial TEM observations were a first step to a better morphofunctional understanding, but at present CSLM coupled to 3D reconstruction appears to be the most reliable and accurate technique (Ventura and Castano 1977; Castano and Ventura 1978,1979; Shotton 1989; Mayhew 1992; Parazza et al. 1993).

Our 3D reconstructions are consistent with the results of Cauna (1956b) who stated that the nerve fiber, after having lost its myelin sheath on entry to the corpuscle, branches repeatedly without interconnections along its course. Despite the high image resolution, analysis was sometimes difficult, but in case of doubtful or difficult interpretation, elimination of one fluorescence channel (Figures 2C and 2D) reduced image complexity and enhanced anatomic analysis. However, it is impossible to be sure of complete marking of the neural structure, owing to the thickness of the sample and to random impregnation by antibodies. In addition to a possible anatomic interruption, nerve discontinuities can also be explained by the fact that thin regions, which may be poorer in neurofilaments, are less reactive to incident light and/or because of high absorption of the reflected light during its course through the skin sample (Cheng and Summers 1990; Carlsson 1991; Rumio et al. 1995b).

According to the labeling technique used, consistent visual differences can exist and image interpretation may become a matter of debate (Ramieri et al. 1992; Castano et al. 1995; Navarro et al. 1995). Comparing two labels, Rumio et al. (1995a) reported in a confocal study that the flattened and discoidal portions identified along the nerve course within the corpuscle looked different. With a PGP 9.5 label these regions appeared discoidal, and silver impregnation (Winkelmann technique) revealed them as slightly dilated segments or varicose elements that were less visible. The authors stated that these differences in aspect could be explained by the difference of staining mechanisms because these flattened discs and varicosities, which are rich in closely packed mitochondria, are less impregnated by the silver–lipoprotein precipitate that preferentially labels areas rich in neurofilaments. However, these expansions that appear as discoidal areas in TEM reconstructions are probably the same structures that have been identified with CSLM and immunolabeling (Ventura and Castano 1977; Castano and Ventura 1978,1979).

Castano et al. (1995) reported with PGP 9.5 labeling that Meissner corpuscles can present several discoidal formations. However, we identified, from a sample of five (not shown), only one flattened disc per corpuscle with a smaller mean size (Figures 2C and 2D). This difference may be partly explained by the different staining precision between PGP 9.5 (neuroplasm protein) and NF 70-200 (neurofilaments from 70 to 200 kD) or, more probably, by individual variations. Several quantitative and qualitative studies have demonstrated that changes in Meissner corpuscle shape and size, nerve aspects, and lamellar cell organization are common with occupation, gender, aging, or nerve impairment in humans (Cauna 1956b; Bolton et al. 1966; Schimirgk and Rüttinger 1980; Matsuoka et al. 1983). Meissner corpuscles have also been commonly described as multiply (double or more) innervated in humans but our five observations were all simply innervated (not shown) (Cauna 1956b; Cauna and Ross 1960; Munger and Idé 1988; Saxod 1996). According to Matsuoka et al. (1983), 54% of Meissner corpuscles in human fingers are supplied by only one myelinated fiber, and the remainder are connected by two or more.

In 1896, Timofeew described thin accessory fibers accompanying human Meissner corpuscles in dermal papillae (Ruffini 1902; Cauna 1956b). In a primate TEM study, Castano et al. (1991) confirmed the presence of unmyelinated nerve fibers associated with Meissner corpuscles, but in a later human confocal study with PGP 9.5 immunolabeling they were unable to identify this extracorpuscular network. Rumio et al. (1995a) demonstrated thin fibers close to human Meissner corpuscles that were identified as intraepidermal nerve fibers (INFs). According to Björklund et al. (1986), these may be thin sympathetic nerves in the vicinity of Meissner corpuscles on the basis of a neuron-specific enolase-like (NSE-Li) and neurokinin A-like (NKA-Li) immunoreactivity. Several descriptions of such unmyelinated nerve fibers have been given in animal species, but convincing evidence is lacking in humans (Castano 1974; Idé 1976; Castano and Ventura 1978; Munger and Idé 1988; Castano et al. 1991). Despite the fact that very thin fibers of less than 0.8 μm in diameter can be isolated with CSLM,

the interweaving of the nerve and lamellar cells shows successive identified layers. At left, the nerve component appears larger, perhaps because the section passes through a flattened area. Lens 40/1.30. Bar = 15 μm. (**D**) Confocal (CSLM, laser argon 488 nm) image of Meissner corpuscles labeled by fluorescent-conjugated antibodies against NF 70-200 (yellow-green) and PS-100 (red). The afferent nerve fiber branches into two separate corpuscles localized in a single dermal papilla. We interpret the areas lacking lamellar cell labeling as the nuclei. Measurement of the largest corpuscle yields 23 μm diameter and 40 μm length. Ray casting reconstruction technique. Lens 40/1.30. Bar = 25 μm.

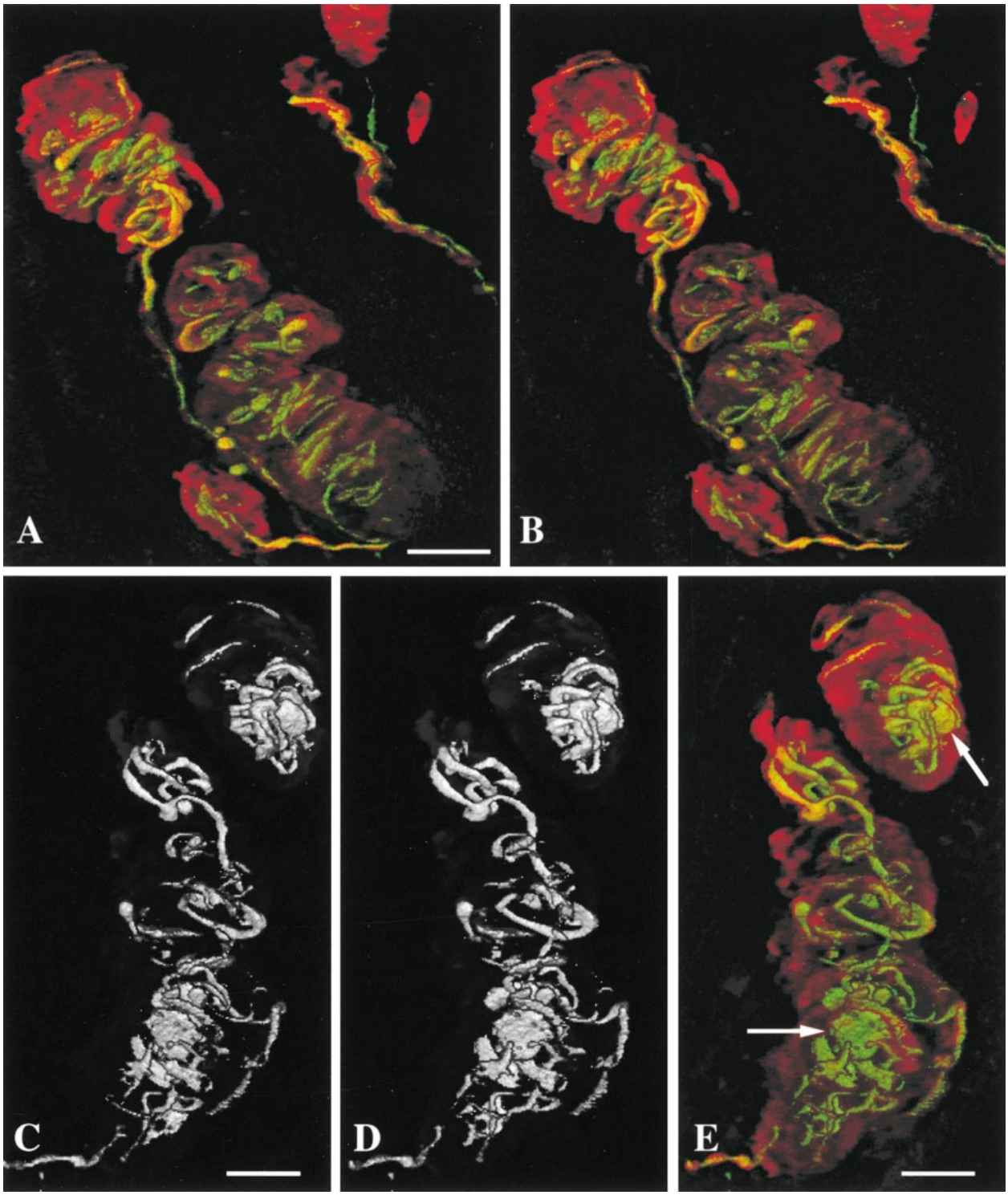

Figure 2 (**A,B**) 3D reconstruction of Meissner corpuscles labeled by fluorescent-conjugated antibodies against NF 70-200 (yellow-green) and PS-100 (red) obtained from 50 1-μm serial optical sections (CSLM, laser argon 488 nm). **B** is 15° right rotated with respect to **A**. Three corpuscles are innervated by a single afferent nerve fiber. Interrupted regions along the nerve course are probably due to lack of labeling or incomplete photonic reflection. Reconstructed volume of 512 × 512 × 80 voxels (1 voxel = 0.3 μm on a side). Stereoscopic pairs setup for cross-eyed viewing. Ray casting reconstruction technique. (**C,D**) Stereoscopic images of 3D reconstruction of Meissner corpuscles labeled by fluorescent-conjugated antibodies against NF 70-200 (yellow-green) and PS-100 (red) obtained from 50 1-μm serial optical sections (CSLM, laser argon 488 nm). This image is the same as **A** and **B**, with a rotation of 40° along the longitudinal axis. **D** is 15° right rotated with respect to **C**. The FITC (NF 70-200) signal has been taken into consideration alone to facilitate interpretation. The extra and intracorpuscle nerve

optical resolution limits may be one explanation of their absence in our reconstructions (Carlsson 1991). Nevertheless, the fact that neither of the antibodies against NF 70-200 and PGP 9.5 specific for myelinated and nonmyelinated fibers applied in the present and other confocal studies showed any thin extracorpuscular neural network does cast a serious doubt on its existence (Castano et al. 1995; Rumio et al. 1995a).

In addition to the neural component, lamellar cells are another important part whose functional role is not yet completely understood. They are considered to be Schwann cell derivatives because they are labeled by specific Schwann cell markers (Iwanaga et al. 1982; Hachisuka et al. 1984; Munger and Idé 1988; Saxod 1996; Vega et al. 1996). The cell membranes are in close contact with the nerve fiber all along its course, but this complex stacking is sometimes difficult to interpret even on a clearly bi-colored 3D reconstruction (Figures 2A and 2B). Cauna and Ross (1960) showed that the nerve endings enter into a close appositional relationship with the flattened portions of lamellar cells and, in some instances, the cell and axolemmal membranes are thickened, with small packed vesicles on both sides. TEM descriptions have shown axonal spines along the longitudinal axis of the axon, microvesicules resembling synaptic vesicles, consistently electron-opaque membranes, localized Ca^{2+} in terminal axoplasm, and a concentration of packed mitochondria in nerve expansions (Cauna and Ross 1960; Haschimoto 1973; Castano 1974; Munger and Idé 1988; Tachibana et al. 1992). This particular intimate relationship between these flattened discoidal expansions and lamellar cells plausibly argues in favor of a transduction process during mechanical stress of the corpuscle at this level.

Acknowledgments

We wish to thank Dr F. Labat–Moleur MD for technical assistance, Prof F. Moutet (Hand Surgery Unit at Grenoble University Hospital, France) who provided us with human samples, and Prof J. Carlsson for his translation contribution.

Literature Cited

Björklund H, Dalsgaard CJ, Jonsson CE, Hermasson A (1986) Sensory and autonomic innervation of non-hairy and hairy human skin. An immunohistochemical study. Cell Tissue Res 243:51–57

Bolton CF, Winkelmann RK, Dyck PJ (1966) A quantitative study of Meissner's corpuscles in man. Neurology 16:1–9

Breatnach AS (1977) Electron microscopy of cutaneous nerves and receptors. J Invest Dermatol 69:8–26

Carlsson K (1991) The influence of specimen refractive index, detector signal integration, and non-uniform scan speed on the images properties in confocal microscopy. J Microsc 163:167–178

Castano P (1974) Further observations on the Wagner-Meissner's corpuscle of man. An ultrastructural study. J Submicrosc Cytol 6:327–337

Castano P, Marcucci A, Miani A Jr, Morini M, Veraldi S, Rumio C (1993) Central and peripheral nervous structures as seen at the confocal scanning laser microscope. J Microsc 175:229–237

Castano P, Rumio C, Morini M, Miani A Jr, Castano SM (1995) Three-dimensional reconstruction of the Meissner's corpuscle of man after silver impregnation and immunofluorescence with PGP 9.5 antibodies using confocal scanning laser microscopy. J Anat 186:261–270

Castano P, Ventura RG (1978) The Meissner's corpuscle of the green monkey. (*Cercopithecus aetiops L.*). I. The organization of nervous component. J Submicrose Cytol 10:327–344

Castano P, Ventura RG (1979) The Meissner's corpuscle of the green monkey (*Cercopithecus aetiops L.*). II. The connective tissue components. Some considerations from a functional standpoint. J Submicrose Cytol 11:185–191

Castano P, Ventura RG, Maddalone M (1985) Notes on morphofunctional differences between the Meissner's corpuscles of man and the green monkey (*Cercopithecus aetiops L.*). Folia Morphol 33:294–298

Castano P, Ventura RG, Pizzini G, Marcucci A, Morini M (1991) Unmyelinated nerve fibers associated with Meissner's corpuscle in the green monkey (*Cercopithecus aetiops L.*). Funct Dev Morphol 1:51–54

Cauna N (1956a) Structure and origin of the capsule of Meissner's corpuscles. Anat Rec 124:77–92

Cauna N (1956b) Nerve supply and nerve endings in Meissner's corpuscles. Am J Anat 99:315–327

Cauna N, Ross LL (1960) The fine structure of Meissner's touch corpuscles of human fingers. J Biophys Biochem Cytol 8:467–482

Cheng PC, Summers RG (1990) Image contrast in confocal light microscopy. In Pawley JB, ed. Handbook of Biological Confocal Microscopy. New York, Plenum Press, 179–195

Chouchkov ChN (1973) Further observations of the fine structure of Meissner's corpuscles in human digital skin and rectum. Z Mikrosk Anat Forsch 87:33–45

Dalsgaard CJ, Björklund H, Jonsson CE, Hermasson A, Dahl D (1984) Distribution of neurofilament-immunoreactive fibers in human skin. Histochemistry 81:111–114

Dubövy P, Rosario CM, Aldsögius H (1993) Combination of nonspecific cholinesterase histochemistry and immunofluorescence staining for the study of the sensory innervation of skin and muscle. Histochem J 25:112–118

Hachisuka H, Mori O, Sakamoto F, Sasai Y, Nomura H (1984) Immunohistochemical demonstration of S-100 protein in the cutaneous nervous system. Anat Rec 210:639–646

Halata Z (1975) The mechanoreceptors of the mammalian skin. Ultrastructure and morphological classification. In Brodal A, Hild W, van Limborgh J, Ortmann R, Schlieber TH, Töndury G, Wolff E, eds. Advances in Anatomy, Embryology and Cell Biology. Vol 50. Fasc 5. Berlin, Springer-Verlag, 20–26

course is clearly individualized and dilated flat expansions are noticeable along the nerve course in two corpuscles. At the inferior part of the larger corpuscle, the afferent nerve fiber gives at least two intracorpuscular branches. Stereoscopic pairs setup for cross-eyed viewing. Ray casting reconstruction technique. (**E**) 3D reconstruction of Meissner corpuscles labeled by fluorescent-conjugated antibodies against NF 70-200 (yellow-green) and PS-100 (red) obtained from 50 1-μm serial optical sections (CSLM, laser argon 488 nm). The image has been rotated 40° along the longitudinal axis according to **A** and **B**. Discoidal and fringed regions (arrows) are clearly evident along the nerve course through two corpuscles, with a mean diameter of 15 ± 1 μm. Ray casting reconstruction technique. Lens 40/1.30. Bars = 20 μm.

Haro JJ, Vega JA, Del Valle ME, Calzada B, Zaccheo D, Malinovsky L (1991) Immunohistochemical study of sensory nerve formations in human glabrous skin. Eur J Morphol 29:271–284

Haschimoto K (1973) Fine structure of the Meissner's corpuscle of human palmar skin. J Invest Dermatol 60:20–28

Idé C (1976) The fine structure of the digital corpuscle of the mouse toe pad, with special references to nerve fibers. Am J Anat 147:329–356

Iggo A (1974) Cutaneous receptors. In Hubbard JI, ed. Peripheral Nervous System. New York, Plenum Press, 347–404

Iwanaga T, Fujita T, Takahashi Y, Nakajima T (1982) Meissner's and Pacinian corpuscles as studied by immunohistochemistry for S-100 protein, neuron-specific enolase and neurofilament protein. Neurosci Lett 31:117–121

Karanth SS, Springall DR, Kuhn DM, Levene MM, Polak JM (1991) An immunohistochemical study of cutaneous innervation and the distribution of neuropeptides and protein gene product 9.5 in man and commonly employed laboratory animals. Am J Anat 191:369–383

Kennedy WR, Wendelschafer–Crabb G (1993) The innervation of human epidermidis. J Neurol Sci 115:184–190

Matsuoka S, Suzuki H, Morioka S, Ogawa Y, Kojima T (1983) Quantitative and qualitative studies of Meissner's corpuscles in human skin with special reference to alterations caused by aging. J Dermatol 10:205–216

Mayhew TM (1992) A review of recent advances in stereology for quantifying neural structure. J Neurocytol 21:313–328

Munger BL, Idé C (1988) The structure and function of cutaneous sensory receptors. Arch Histol Cytol 51:1–34

Navarro X, Verdü E, Wendelschafer–Crabb G, Kennedy WR (1995) Innervation of cutaneous structures in the mouse hind paw: a confocal microscopy immunohistochemical study. J Neurosci Res 41:111–120

Parazza F, Humbert C, Usson Y (1993) Method for 3D volumetric analysis of intranuclear fluorescence distribution in confocal microscopy. Comp Med Imag Graph 17:189–200

Ramieri G, Stella M, Calcagni M, Teich-Alesia S, Cellino G, Panzica GC (1992) Morphology of corpuscular receptors in hairy and non-hairy human skin as visualized with an antiserum to protein gene product 9.5 compared to antineuron-specific enolase and anti S-100 protein. Acta Anat 144:343–347

Rigaut JP, Vassy J (1991) High-resolution three-dimensional images from confocal scanning laser microscopy. Anal Quant Cytol Histol 13:223–232.

Ruffini A (1902) Sull` apparato nervoso di Timofeew od apparato ultraterminale nei corpuscoli di Meissner della cute umana. Biblio Anat 11:267–281

Rumio C, Castano P, Veraldi S, Morini M, Castano M (1995a) The innervation of human skin studied with confocal scanning laser microscopy: a comparison between PGP 9.5 immunofluorescence and silver impregnation. Neuroimage 2:102–111

Rumio C, Morini M, Miani A Jr., Barajon I, Castano P (1995b) A simple method for overcoming some problems when observing thick reflective biological samples with a confocal scanning laser microscope. J Microsc 177:85–89

Saxod R (1996) Ontogeny of the cutaneous sensory organs. Microsc Res Tech 34:313–333

Schimirgk K, Rüttinger H (1980) The touch corpuscles of plantar surface of the big toe. Histological and histometrical investigations with respect to age. Eur Neurol 19:49–60

Shotton MD (1989) Confocal scanning optical microscopy and its applications for biological specimens. J Cell Sci 94:175–206

Stefansson K, Wollman RL, Moore BW (1982) Distribution of S-100 protein outside the central nervous system. Brain Res 234: 309–317

Tachibana T, Nawa T, Mizuhira V, Yoshida Y (1992) Ultrastructural localization of calcium in mechanoreceptors of the oral mucosa. J Neurocytol 21:745–753

Timofeew D (1896) Über eine besondere Art von eingekapselten Nervenendigungen in den männlichen Geschlechtsorganen bei Säugetieren. Anat Anz 11:44–49

Vega JA, Llamosas MM, Huerta JJ, García–Fernández JM (1996) Study of human cutaneous sensory corpuscles using double immunolabeling and confocal laser scanning microscopy. Anat Rec 246:557–560

Ventura RG, Castano P (1977) Meissner's corpuscle of the green-monkey. Electron microscope three-dimensional reconstruction and quantitative analysis of the nervous supply. Acta Anat 99:312